

# Three arginine residues in apolipoprotein A-I are critical for activation of lecithin:cholesterol acyltransferase

Stein Roosbeek,\* Berlinda Vanloo,\* Nicolas Duverger,<sup>§</sup> Hans Caster,\* Joke Breyne,\* Iris De Beun,\* Hetal Patel,\*\* Joël Vandekerckhove,<sup>†</sup> Carol Shoulders,\*\* Maryvonne Rosseneu,<sup>1,\*</sup> and Frank Peelman\*

Laboratory for Lipoprotein Chemistry,\* Department of Biochemistry, Ghent University, B-9000 Ghent, Belgium; Department of Medical Protein Research,<sup>†</sup> Flanders Interuniversity Institute for Biotechnology, B-9000 Ghent, Belgium; Aventis,<sup>§</sup> Vitry-sur-Seine 94403, France; MRC Molecular Medicine Group,\*\* Clinical Sciences Centre, Hammersmith Hospital, London W12 0NN, UK

**Abstract** Previous studies have suggested that the helical repeat formed by residues 143–164 of apolipoprotein A-I (apoA-I) contributes to lecithin:cholesterol acyltransferase (LCAT) activation. To identify specific polar residues involved in this process, we examined residue conservation and topology of apoA-I from all known species. We observed that the hydrophobic/hydrophilic interface of helix 143–164 contains a cluster of three strictly conserved arginine residues (R149, R153, and R160), and that these residues create the only significant positive electrostatic potential around apoA-I. To test the importance of R149, R153, and R160 in LCAT activation, we generated a series of mutant proteins. These had fluorescence emission, secondary structure, and lipid-binding properties comparable to those of wild-type apoA-I. Mutation of conserved residues R149, R153, and R160 drastically decreased LCAT activity on lipid-protein complexes, whereas control mutations (E146Q, D150N, D157N, R171Q, and A175R) did not decrease LCAT activity by more than 55%. The markedly decreased activities of mutants R149, R153, and R160 resulted from a decrease in the maximal reaction velocity  $V_{max}$  because the apparent Michaelis-Menten constant  $K_m$  values were similar for the mutant and wild-type apoA-I proteins. These data suggest that R149, R153, and R160 participate in apoA-I-mediated activation of LCAT, and support the “belt” model for discoidal rHDL. In this model, residues R149, R153, and R160 do not form salt bridges with the antiparallel apoA-I monomer, but instead are pointing toward the surface of the disc, enabling interactions with LCAT.—Roosbeek, S., B. Vanloo, N. Duverger, H. Caster, J. Breyne, I. De Beun, H. Patel, J. Vandekerckhove, C. Shoulders, M. Rosseneu, and F. Peelman. Three arginine residues in apolipoprotein A-I are critical for activation of lecithin:cholesterol acyltransferase *J. Lipid Res.* 2001. 42: 31–40.

**Supplementary key words** HDL • enzyme • lipoprotein • cholesterol

The role of apolipoprotein A-I (apoA-I) in the metabolism and maturation of different subclasses of high density lipoproteins (HDL) has been well documented (1). ApoA-I is synthesized as a prepropeptide, and is cleaved in plasma

to a 243-amino acid residues protein. ApoA-I associates with phospholipids and cholesterol, and acts as acceptor of cellular lipids to promote “reverse cholesterol transport” (2). In this process, lipid-free apoA-I “solubilizes” cellular lipids through a direct interaction with the donor plasma membrane, or specific receptors, such as the scavenger receptor class B type I (SR-BI) receptor (3) and the adenosine triphosphate (ATP)-binding cassette transporter ABCA1 (4–6). ApoA-I also mediates the maturation of HDL through the activation of lecithin:cholesterol acyltransferase (LCAT). LCAT converts cholesterol to cholesteryl esters (7), through the hydrolysis of the *sn*-2 fatty acid of lecithin and esterification of the hydroxyl group of cholesterol. The cholesteryl esters are incorporated into the core of HDL, and exchanged with either low density lipoprotein (LDL) or very low density lipoprotein lipids, or taken up by the liver through the action of the SR-BI receptor (3).

ApoA-I has been sequenced both at the protein and cDNA level (8, 9), and the occurrence of 11- and 22-residue helical repeats has been predicted by internal homology calculations (10). These bind lipids and have a unique amphipathic character, with separate hydrophilic and hydrophobic faces (11). A crystal structure for lipid-free apoA-I, apoA(1–43)A-I, has been determined at 4-Å resolution (12). ApoA-I forms a nearly continuous nonplanar amphipathic helix, with dimensions of 125 × 80 × 40 Å, in the shape of a horseshoe. The structure comprises 10

Abbreviations: apo, apolipoprotein; apoA(1–43)A-I, lipid-free apoA-I; DMPC, 1,2-dimyristoyl-*sn*-glycero-3-phosphatidylcholine; HDL, high density lipoprotein; HPLC, high performance liquid chromatography; LCAT, lecithin:cholesterol acyltransferase; LDL, low density lipoprotein; PCR, polymerase chain reaction; PLPC, 1-palmitoyl-2-linoleoyl-*sn*-glycero-3-phosphatidylcholine; rHDL, reconstituted high density lipoprotein; SDS-PAGE, sodium dodecyl sulfate-polyacrylamide gel electrophoresis; SR-BI, scavenger receptor class B type I.

<sup>1</sup> To whom correspondence should be addressed.

helical segments, named A1–A10, which are punctuated by small or pronounced kinks at regularly spaced proline residues. In the unit cell of the crystal, four apoA-I monomers form two antiparallel dimers that are associated via their hydrophobic faces. Such a structure is predicted to be conserved in lipid-associated apoA-I, as the dimensions of the dimer are compatible with those of discoidal and spherical HDL (12).

Two general models have been proposed for discoidal nascent HDL, the preferred substrate for LCAT. The “belt” model, proposed by Segrest et al. (13), consists of an apoA-I dimer made of two antiparallel monomers. These monomers surround the edge of the disc and are oriented parallel to the face of the discoidal particle. This is reminiscent of the “horseshoe” structure of crystalline apoA-I. In the alternative “picket-fence” model proposed by Brassier et al. (14) and by Phillips et al. (15), the helical repeats are oriented perpendicular to the faces of the disc, and are parallel to the phospholipid acyl chains. This model is supported by attenuated total reflection infrared measurements, performed on a Ge plate (14, 16), whereas the belt model is favored by infrared measurements at an air-water interface (17).

Previous studies have suggested that helical repeats 6 and 7 of apoA-I are critical for the activation of LCAT by apoA-I, but the specific residues that mediate this activation have not been identified. Thus, it is well established that monoclonal antibodies directed against residues 143–164 of apoA-I suppress the activation of LCAT by apoA-I, while synthetic peptides that encompass helical repeats 6 and 7 activate LCAT. Conversely, the activation of LCAT by apoA-I is impaired by naturally occurring or genetically engineered apoA-I proteins that lack helical repeat 6 and 7. Sorci-Thomas et al. (18) have further demonstrated that rotation of the hydrophobic face of helix 143–164 of apoA-I by about 80° markedly reduces LCAT activation. Finally, this region of apoA-I harbors three naturally occurring missense mutations, R151C, R160L, and H162Q, associated with decreased LCAT activation.

In the present study, we have used the crystal structure of apoA-I, comparative sequence analysis, and site-directed mutagenesis to address the issue of LCAT activation by apoA-I. We demonstrate that helical repeat 6 contains a cluster of three strictly conserved arginine residues (Arg-149, Arg-153, and Arg-160), and that these are critical for LCAT activation. Importantly, the data provide experimental support for the belt model conformation of discoidal HDL.

## MATERIALS AND METHODS

### Sequence analysis and computer modeling

The electrostatic potential calculations were performed on monomer A in the crystalline structure of apo( $\Delta$ 1–43)A-I (12), using the Delphi program (19), as implemented in the MSI Insight97 software package (Molecular Simulations, San Diego, CA). Calculations were performed with actual atomic charges, as defined by the CHARMM atomic force field (20), a dielectric constant of 8 for the solute, and 80 for the solvent. A focusing approach was used to reduce grid boundary effects, where the

monomer filled 23% of a  $63 \times 63 \times 63$  points grid, during the first coarse calculation, and 80% of the  $63 \times 63 \times 63$  points grid in the focusing calculation.

Sequences of human (P02647), cynomolgus monkey (P15568), pig (P18648), cow (P15497), dog (P02648), rabbit (P09809), tree shrew (O18759), mouse (Q00623), rat (P04639), golden hamster (Q9Z2L4), hedgehog (Q9TS49), chicken (P08250), quail (P32918), and duck (O42296) apoA-I were aligned by CLUSTAL W (21), available at <http://www.ebi.ac.uk/clustalw/>.

For sequence comparison between the helices of human apoA-I, apoA-IV, apoA-II, apoE, apoC-I, apoC-II, and apoC-III, these sequences were divided in overlapping stretches of 36 residues, which were displayed in a helical wheel projection.

### Site-directed mutagenesis

Polymerase chain reaction (PCR) and the appropriate restriction sites were used to manipulate the apoA-I sequence. Mutagenesis was performed by a two-step PCR-based strategy using *Pfu* DNA polymerase in accordance with the manufacturer's instructions (Stratagene, UK). The template was the plasmid pALTER/apoA-I, which encompasses nucleotides 1887–2292 of the apoA-I sequence (GenBank accession number J0098). To facilitate cloning, the *Sst*I site at nucleotides 1923–1928 of apoA-I was mutated; this did not alter the encoded sequence. The first-round PCRs were performed with a forward mutagenic oligonucleotide >35 bases in length. The sequence of the reverse oligonucleotide was 5'-GACTATGGATCCTCACTGGGTGTTGAGCTTCTT-3'. The sequence of the forward primer for the second-round PCR was 5'-AGATGGAGCTCTACCGCCAGAAGGTGGAGCCGCTGCGCGCAGAACTGCAAGAGGGCGCGGCCAG-3'. The reverse primer was the product of the first-round PCR. The mutant apoA-I cDNAs were introduced into the PXL2769.apoA-I vector (22). The sequences of all constructs were confirmed.

### Expression and purification of the recombinant proteins

The expression system under the control of the T7 promoter had been described previously for apoA-IV (22). The expression vector pXL2769 for wild-type apoA-I, and the corresponding vectors for the apoA-I mutants, were introduced into *Escherichia coli* BL21(DE3) pLysS cells, for expression of histidine-tagged apoA-I mutants. Bacteria were grown overnight at 37°C in Terrific Broth medium, supplemented with ampicillin (100  $\mu$ g/ml) and chloramphenicol (50  $\mu$ g/ml). Five milliliters of this culture was used to inoculate 1 liter of the same medium. Cultures were grown at 37°C until an absorbance at 610 nm of about 0.7 was reached. Isopropyl- $\beta$ -D-thiogalactoside was then added to a final concentration of 1 mM, followed by a 15-min incubation at 30°C to induce apoA-I expression. Rifampicin was added to a concentration of 100  $\mu$ g/ml, and the cells were incubated for 60 min, harvested by centrifugation, and frozen at –20°C. ApoA-I expression was verified by sodium dodecyl sulfate-polyacrylamide gel electrophoresis (SDS-PAGE).

For protein extraction, the pellets were resuspended by addition of 5 ml of a 100 mM sodium phosphate lysis buffer, pH 7.4, containing 1 mM phenylmethylsulfonyl fluoride per gram of bacteria. The cells were disrupted by five 5-min cycles of sonication at 70 W, using a Vibracell™ sonifier (Sonic, Newtown, CT). Whole cells and cellular debris were removed by centrifugation at 2,000 *g* for 15 min at 4°C, in an Eppendorf centrifuge. Nucleic acids were precipitated by addition of 10 ml of a 100 *g*/l solution of streptomycin sulfate, per gram of bacterial protein in the supernatant fraction. The mixture was incubated overnight at 4°C, and centrifuged at 6,000 *g* for 15 min at 4°C in an Eppendorf centrifuge, to remove the precipitated material.

The apoA-I proteins were purified in the supernatant by affinity chromatography on a Ni-Probond column (InVitrogen, San Diego,

CA), equilibrated in a 100 mM phosphate buffer, pH 8.0, containing 6 M guanidium hydrochloride. The wild-type and mutant apoA-I proteins were eluted from the column by a stepwise decrease in the elution buffer pH, from 8.0 down to 6.0, 5.0, and 4.0. The eluted fractions were tested for the presence of apoA-I protein by SDS-PAGE. The fractions eluting at pH 4.0, containing pure apoA-I, were dialyzed against a 5 mM  $\text{NH}_4\text{HCO}_3$  buffer and lyophilized.

### Preparation and isolation of the apolipoprotein-lipid complexes

Reconstituted HDL (rHDL) consisting of 1-palmitoyl-2-linoleoyl-phosphatidylcholine/cholesterol/apoA-I at a ratio of 2:0.1:1 (w/w/w) were prepared by the cholate dialysis method (23). The homogeneity and yield of the reconstituted HDL were tested by separation on a Superose 6PG column equilibrated in a 10 mM Tris-HCl buffer, pH 8.0, containing 150 mM NaCl in a fast protein liquid chromatography system. Composition and size determination was performed on the top fractions of the elution peak of the complex. The lipid and apolipoprotein compositions of the complexes were obtained by an enzymatic colorimetric assay for phospholipid and cholesterol (bioMérieux, Charouneries-les-Bains, France; Boehringer, Mannheim, Germany) and by protein quantification of apoA-I by phenylalanine assay by high performance liquid chromatography (HPLC) (24).

### Physicochemical characterization of the reconstituted HDL

The intrinsic fluorescence of the tryptophan residues of apoA-I wild-type and mutants, either lipid free or in rHDL complexes, was measured with an AMINCO-Bowman series 2 spectrofluorimeter (Spectronic Unicam, Rochester, NY) at an excitation wavelength of 280 nm, with 4-nm excitation and emission slit widths. Spectra were recorded between 310 and 450 nm. The maximal wavelengths of tryptophan fluorescence emission were calculated from the corrected spectra.

Circular dichroism spectra of the apoA-I mutants and their rHDL complexes were measured on a JASCO (Tokyo, Japan) 710 spectropolarimeter at wavelengths between 186 and 250 nm. Measurements were carried out at a protein concentration of 50  $\mu\text{g}/\text{ml}$  in a 0.01 M sodium phosphate buffer, pH 7.4. Nine spectra were collected and averaged for each sample. The secondary structure was estimated by curve fitting with the Circular Dichroism Deconvolution by back propagation Neural Networks program (25).

### Production of wild-type rLCAT in BHK cells

Recombinant LCAT was produced by a baby hamster kidney (BHK) cell line, stably transfected with the LCAT cDNA, under control of the mouse metallothionein promoter (26). Stably transfected BHK cells were incubated with Dulbecco's modified Eagle medium (DMEM; GIBCO-BRL, Gaithersburg, MD) containing 10% fetal bovine serum, streptomycin (100  $\mu\text{g}/\text{ml}$ ), and penicillin (100 units/ml). After 48 h, the confluent cells were washed with Opti-MEM and the DMEM was replaced by serum-free Opti-MEM (GIBCO-BRL). After 48 h of incubation the medium was collected, filtered through a 0.22- $\mu\text{m}$  pore size filter (Millipore, Bedford, MA), and dialyzed against 20 mM Tris-HCl buffer, pH 8.0. The rLCAT was purified on a Resource<sup>TM</sup> Q HR column (Pharmacia, Uppsala, Sweden) with a NaCl gradient between 0 and 500 mM. rLCAT was collected in 1-ml fractions and stored at  $-80^\circ\text{C}$ , at a concentration of about 150  $\mu\text{g}/\text{ml}$ .

### LCAT activation properties of the rHDL complexes

The activity of the LCAT enzyme with the various rHDL complexes as substrates was determined by measuring the amount of cholesteryl esters, generated during the enzymatic reaction, by HPLC (27).

The initial velocities were determined in the linear portion of the curves, that is, between 0 and 25% cholesteryl ester formation. The assay mixture consisted of variable amounts of rHDL complexes at cholesterol concentrations varying between 2 and 20  $\mu\text{M}$ , defatted bovine serum albumin (4 mg/ml; Sigma, St. Louis, MO), and 6 mM 2-mercaptoethanol. Tris-HCl buffer (0.01 M, pH 8.0), 0.15 M NaCl, 0.3 mM  $\text{Na}^+$ -ethylenediaminetetraacetic acid, and 1 mM  $\text{NaN}_3$  were added to a final reaction volume of 0.5–1.5 ml. Complexes were preincubated for 20 min at  $37^\circ\text{C}$ , before addition of 50–150  $\mu\text{l}$  of BHK rLCAT, to initiate the enzymatic reaction. The reaction was performed at  $37^\circ\text{C}$ , and it was stopped by extraction of the incubation mixture with hexane-isopropanol 3:2 (v/v), containing cholesteryl heptadecanoate (Sigma) as an internal standard, for cholesteryl ester quantification.

HPLC separation and quantification of the cholesteryl esters were carried out as described previously (27). The apparent kinetic parameters  $V_{max}$  and  $K_m$ , together with the estimated error on the parameters, were determined for each apoA-I/rHDL complex. These values were calculated by fitting the initial velocity  $V_0$ , as a function of the cholesterol concentration, to the Michaelis-Menten equation, using the SigmaPlot software (SPSS, Chicago, IL).

## RESULTS

### Selection of the mutants

The electrostatic potential around an apoA-I monomer is predominantly negative (Fig. 1). The exception is a positive electrostatic potential around the arginine cluster R149, R153, and R160 of helix 6, and around residues R171 and K182 of helix 7. We examined the conservation and location of these arginine residues in all known apoA-I sequences of different species. The Edmundson wheel representation of eight helical repeats is shown in Fig. 2, for human, cynomolgus monkey, pig, cow, dog, rabbit, tree shrew, mouse, rat, golden hamster, hedgehog, chicken, quail, and duck apoA-I (28). There is high sequence conservation among apoA-I of the different species, and the amphipathic character of all helices is especially well conserved. A specific feature of the repeat at residues 145–162 is clearly demonstrated in Fig. 2, as the hydrophilic face of this amphipathic helix is characterized by a cluster of three arginine residues at positions 149, 153, and 160. These residues, which account for the positive electrostatic potential described above, are totally conserved among the different species. This cluster of three adjacent arginine residues on the Edmundson wheel representation is unique to helix 145–162, as repeats 101–118, 123–140, and 189–206 have only two adjacent lysines, which are not perfectly conserved among the different species (Fig. 2). A close inspection of the repeats of apoA-IV, apoA-II, apoE, apoC-I, apoC-II, and apoC-III did not reveal any similar cluster of three arginine residues either (data not shown). In the crystal structure of an apoA-I dimer, consisting of two antiparallel monomers, helix 143–164 interacts with repeat 99–120 of the other monomer (Fig. 3). R149, R153, and R160 are not part of the dimer interface and cannot interact with the other repeat. The same holds true for the belt model of an rHDL particle proposed by Segrest et al. (13).



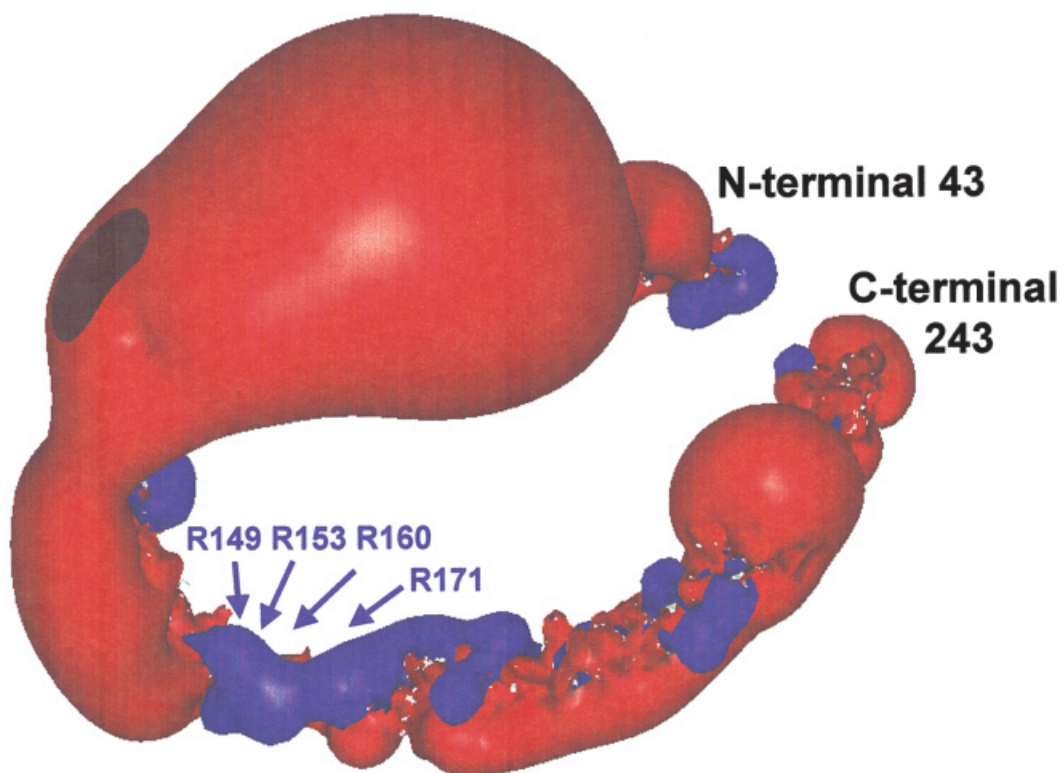


**Fig. 1.** Electrical potentials around a molecule of apoA-I( $\Delta$ 1–43), calculated by the Delphi program on the basis of the coordinates of Borhani and co-workers (12). Red, negative potential at  $-1$  kt/e; blue, positive potential at  $+0.5$  kt/e.

To test the contribution of residues R149, R153, and R160, and of the electrostatic potential around the 22-residue repeats 143–164 and 165–186 of apoA-I to LCAT activation, we constructed the mutants listed in **Table 1**. R149, R153, and R160 were mutated to glutamine, either as single, double, or triple mutants. In addition, acidic residues E146, D150, and D157, which might form ionic interactions with R149, R153, and R160 to stabilize the helical structure, were mutated to a glutamine or an asparagine (Table 1). The requirement for an arginine residue at position 153 was tested by the R153K substitution. An R171Q mutation was performed to decrease the positive electrostatic potential around repeat 167–184. In addition, A175 was mutated to an arginine, in order to increase the positive potential around this helix.

#### Expression and characterization of the apoA-I mutants

Wild-type and mutant apoA-I proteins were expressed in *E. coli*, and comparable yields were obtained (data not shown). The affinity-purified proteins migrated as a single band on SDS-PAGE, with a molecular weight corresponding to that of apoA-I, carrying the N-terminal histidine tag. The secondary structure of the mutant apoA-I proteins was checked by circular dichroism (Table 1), and the percentages of  $\alpha$  helix,  $\beta$  sheet,  $\beta$  turns, and coil were found to be similar to wild-type apoA-I. The secondary structure is characterized by a high percentage of helical structure and low  $\beta$ -sheet content, in agreement with the crystallized structure of apoA( $\Delta$ 1–43)A-I.

#### Lipid-binding properties of wild-type and mutant apoA-I

The association of plasma, wild-type, and mutant apoA-I with 1,2-dimyristoyl-*sn*-glycero-3-phosphatidylcholine (DMPC) vesicles was followed by turbidity measurements at 325 nm, as a function of temperature. As shown in **Fig. 4**, wild-type recombinant apoA-I, the single mutant R153Q, the double mutant R153Q + R160Q, the triple mutant R149Q + R153Q + R160Q, and the D157N mutant, all reacted similarly with DMPC. Around the transition temperature of DMPC, the large multilamellar vesicles were converted into smaller lipid-protein complexes. We also prepared rHDL particles consisting of 1-palmitoyl-2-linoleoyl-*sn*-glycero-3-phosphatidylcholine (PLPC), cholesterol, and recombinant apoA-I and examined their size and homogeneity (**Fig. 5**). The yield of rHDL formed from the mutant proteins was comparable to that of wild-type apoA-I, and each became fully associated with lipids. No peak of lipid-free apoA-I was detected by sensitive tryptophan fluorescence detection, at an elution volume larger than that of the lipid-apolipoprotein complex. The rHDL particles were about 8 nm in diameter and contained 40–60 mol of phospholipid, 3–5 mol of cholesterol per mole of apoA-I, and two molecules of apoA-I. The size of the complexes was further estimated by native gradient gel electrophoresis, in a 4–20% polyacrylamide gradient. The sizes of complexes from the major protein fraction in the gel were comparable for all apoA-I proteins (**Table 2**).

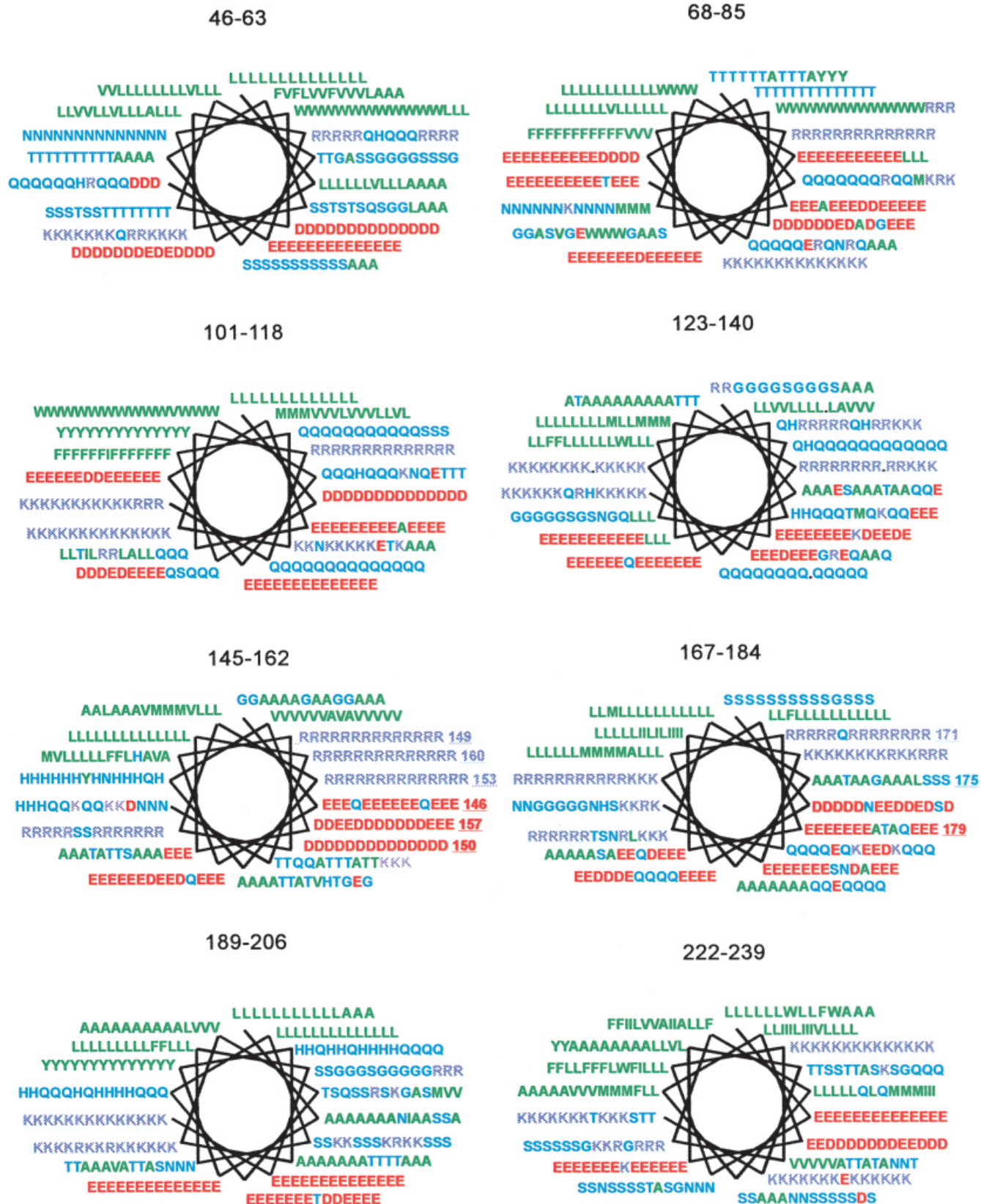


**Fig. 2.** Edmondson wheel representation of 18-residue helical repeats in apoA-I. Residues from left to right: human, cynomolgus monkey, pig, cow, dog, rabbit, tree shrew, mouse, rat, golden hamster, hedgehog, chicken, quail, and duck apoA-I. Red, negative; dark blue, positive; light blue, neutral hydrophilic; green, hydrophobic residues. For convenient graphical representation, the 22-amino acid repeats are truncated by 2 residues at each end.



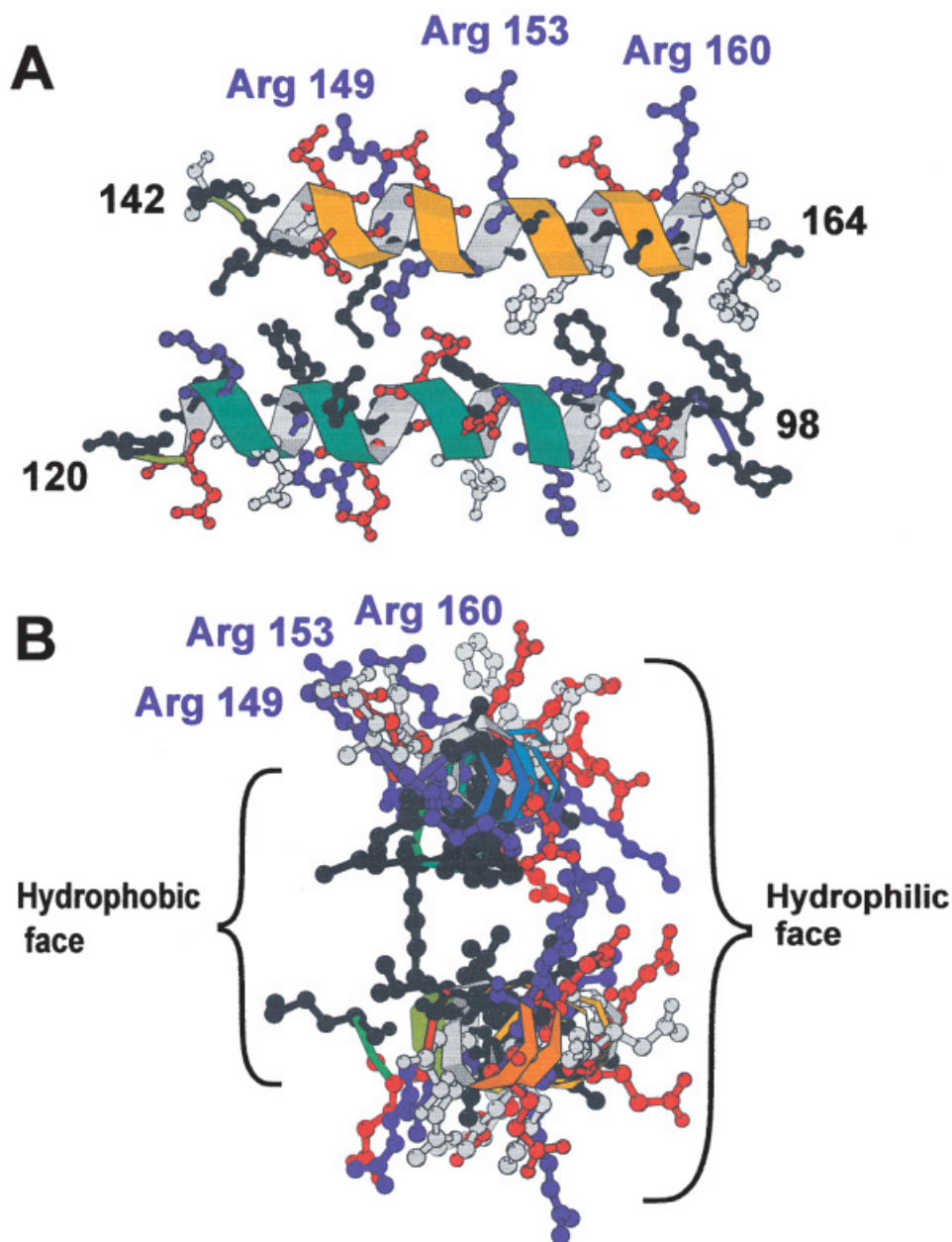


**Fig. 3.** Representation of helix 143–164 of apoA-I in a dimer of apo( $\Delta$ 1–43)A-I, together with the complementary helix 99–120 in the antiparallel dimer. Representation: (A) parallel and (B) perpendicular to the long axis of the helix.

They were relatively small, as they were prepared at a 2:1 (w/w) ratio of phospholipid to protein, to increase the homogeneity of the preparation. Incubation of lipids with wild-type and mutant apoA-I at a 2.5:1 (w/w) ratio yielded a more heterogeneous population of particles (data not shown).

To characterize further the lipid-binding properties of the mutant apoA-I, we measured the maximal wavelength for the tryptophan fluorescence emission of lipid-free apoA-I and rHDL. Consistent with the insertion of the tryptophan residues in apoA-I into a more hydrophobic environment, the tryptophan fluorescence of each apoA-I complex was characterized by a blue shift of 2–3 nm, com-

pared with the lipid-free protein (Table 2). The secondary structure of lipid-bound apoA-I, determined by circular dichroism (Table 1), shows an increased helical content of about 15% for all complexes. This is due to the helix stabilization of the helical repeats by the lipids, accompanied by a decrease of the percentage of coil structure, while  $\beta$ -sheet and  $\beta$ -turn content remain unchanged (Table 1).

#### LCAT activation properties of wild-type and mutant apoA-I

Initial velocity measurements showed a linear increase of up to 20–25% cholesterol esterification in the substrate. All subsequent measurements were carried out within that

TABLE 1. Percentages of secondary structure of apoA-I mutants, lipid-free and in PLPC/cholesterol/apoA-I complexes, determined by circular dichroism

ApoA-I Mutant	Lipid-Free ApoA-I				PLPC/Cholesterol/ApoA-I Complexes			
	$\alpha$ Helix	$\beta$ Sheet	$\beta$ Turn	Coil	$\alpha$ Helix	$\beta$ Sheet	$\beta$ Turn	Coil
	%				%			
Wild type	58	7	14	21	76	3	10	11
R149Q	65	5	13	17	70	4	11	15
R153Q	43	12	16	29	74	3	10	13
R153K	53	8	15	24	68	4	11	17
R160Q	64	5	13	18	74	3	10	13
R149Q + R153Q	61	8	13	18	71	4	11	14
R153Q + R160Q	61	7	14	18	68	4	12	16
R149Q + R153Q + R160Q	57	7	14	22	77	3	10	10
E146Q	39	13	17	31	55	7	13	25
D150N	48	11	15	26	64	5	12	19
D157N	52	10	15	23	61	6	13	20
E146A + R149A	55	6	18	19	66	4	20	11
R149A + D150A	31	18	17	34	77	3	10	10
R153A + D150A	58	7	14	21	79	3	9	9
R171Q	44	11	16	29	65	5	12	18
A175R	30	18	17	35	54	7	14	25

range.  $V_{max}$  and  $K_m$  were determined for wild-type and mutant apoA-I, from  $V_o$  measurements at varying cholesterol concentrations. The parameters were calculated by fitting the experimental data to a Michaelis-Menten equation, using SigmaPlot software (SPSS). Table 3 summarizes the values obtained for  $V_{max}$  and  $K_m$  and the enzymatic efficiency  $V_{max}/K_m$  for wild-type and mutant apoA-I. Compared with wild-type apoA-I, we observed a decreased  $V_{max}$  for all mutants in which one or more residues of the arginine cluster R149, R153, and R160 was mutated to a glutamine. This effect increased with the number of substitutions in the mutant protein. Mutation of a single arginine, either R149, R153, or R160, resulted in a 6- to 10-fold decrease in  $V_{max}$ , compared with a 12- to 25-fold decrease for a double mutant, and a 30-fold decrease for a

triple mutant. Conversely, mutations of acidic residue E146, D150, or D157 had only limited effect, as  $V_{max}$  values were about 50% of wild-type apoA-I. Mutation of both an arginine residue and an acidic residue decreased  $V_{max}$  to a value similar to that of a single arginine mutation, in agreement with the limited effect of mutating an acidic residue of helix 143–160. Surprisingly, substitution of R153 with a lysine residue was almost as deleterious as the R153Q substitution for LCAT activity. Mutation of R171 in the next C-terminal helix had no effect on  $V_{max}$ , while substitution of A175 by an arginine did not affect this parameter either.

The effect of the apoA-I mutations on the dissociation constant  $K_m$  was more limited, as  $K_m$  values were of the same order of magnitude, and varied at most 2- to 3-fold. Calculation of the catalytic efficiency  $V_{max}/K_m$  clearly shows that mutation of one or more arginine residues of the R149, R153, R160 cluster drastically decreases LCAT enzymatic activity on the mutant apoA-I/lipid complexes, to less than 20% of wild-type apoA-I. As the composition, size, and structure of the complexes are comparable, this can be attributed to loss of activation of LCAT by mutation of the cofactor apoA-I.

## DISCUSSION

We have used the crystal structure of apoA-I(1–43), sequence conservation calculations, and sequence alignment programs to detect a unique feature in the hydrophilic face of helix 143–164. This helix had been previously implicated in the activation of LCAT by apoA-I. It contains a cluster of three conserved arginine residues, at matching positions on three turns of this helix. We therefore generated mutations of polar residues in this helix, and measured the biochemical, biophysical, and LCAT activation properties of the mutants. We showed that the secondary structure and lipid-binding properties of the

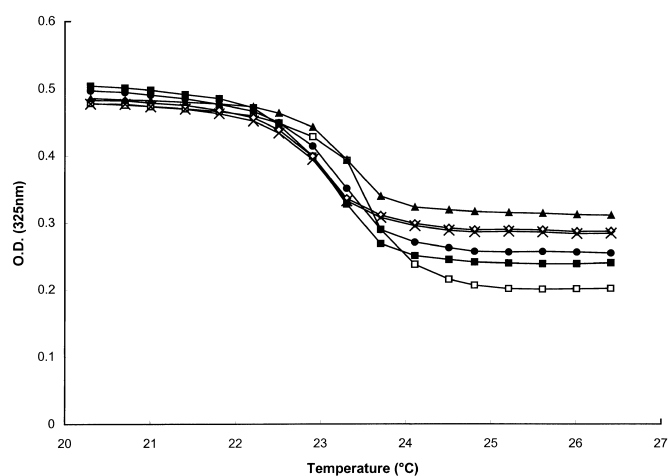
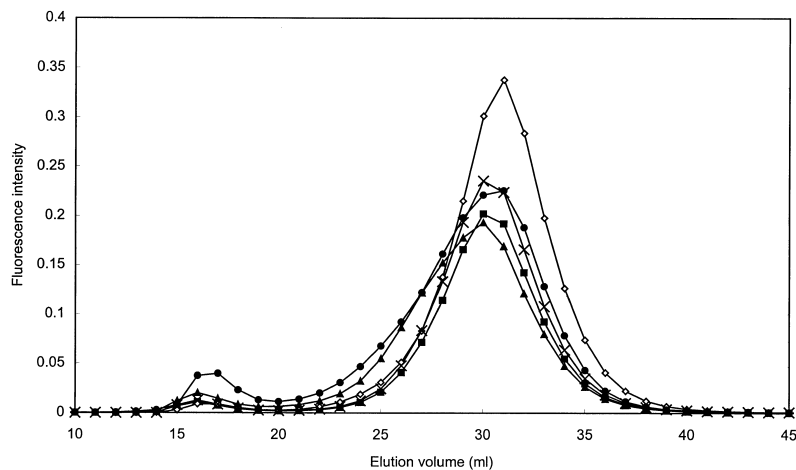


Fig. 4. Turbidity decrease of mixtures of apoA-I mutants with DMPC as a function of temperature, monitored by absorption measurements at 325 nm. Plasma apoA-I (open squares); wild-type apoA-I (solid squares); R153Q mutant (open diamonds); R153Q + R160Q mutant (solid triangles); R149Q + R153Q + R160Q mutant (solid circles); D157N mutant (×).



**Fig. 5.** Elution profiles of PLPC/cholesterol/apoA-I mutants separated on a Superose 6 PG column, monitored by tryptophan fluorescence measurement. Wild-type apoA-I (solid squares); R153Q mutant (open diamonds); R153Q + R160Q mutant (solid triangles); R149Q + R153Q + R160Q mutant (solid circles); D157N mutant (×).

mutants were comparable to those of wild-type apoA-I. Mutations of conserved residues R149, R153, and R160 in helix 6 drastically reduced LCAT activation by the mutants, due to a  $V_{max}$  decrease. In contrast, mutations of acidic residues in this helical repeat, or of R171 in the next C-terminal repeat, did not have such an effect. Taken together, these data suggest that residues R149, R153, and R160 mediate the activation of LCAT by apoA-I.

We have compared the orientation and hydrogen bonding of R149, R153, and R160 in the apo $\Delta(1-43)$ A-I crystal structure, in the belt model proposed by Segrest et al. (13), and in the picket-fence model of Phillips et al. (15). In the belt model, as well as in the crystal structure of apo $\Delta(1-43)$ A-I, R149, R153, and R160 do not form interhelical salt bridges with the corresponding antiparallel repeat 99–120. However, these arginines can form intrahelical salt bridges with E146, D150, and D157. Mutations of the negatively charged residues decreased  $V_{max}$  only by

50%, whereas mutation of any of the conserved arginine residues in helix 143–164 caused a 10-fold decrease of  $V_{max}$ . According to these data, putative intrahelical salt bridges in helix 143–164 would not be critical for the structure and cofactor activity of apoA-I in rHDL. This is suggested by the similar helical content of all mutant proteins, and in addition by the finding that the R153K mutation, which would preserve the potential salt bridge formation between K153 and D150, impairs LCAT activation. In the picket-fence model proposed by Phillips et al. (15), R149, R153, and R160 do not form a cluster of residues, as in the belt model. They are located further apart, as R149 and R160 are at about 20 Å from each other. R153 forms an intrahelical salt bridge with D150, while R149 can form a salt bridge with E179 in the antiparallel helical repeat at residues 165–186. Similarly, D157 and R171 can form an interhelical salt bridge with each other. The decrease in  $V_{max}$  observed with the arginine mutants cannot be due to

**TABLE 2.** Maximal wavelength of tryptophan fluorescence of apoA-I lipid free and in rHDL; diameter and composition of rHDL particles consisting of PLPC/cholesterol/apoA-I

ApoA-I Mutant	$\lambda_{max}$		Diameter		PLPC/ Cholesterol Apo/A-I
	Lipid Free	rHDL	Gradient Gel Electrophoresis	Gel Filtration	
	nm		nm		
Wild type	331	329	7.8	8.0	52/4/01
R149Q	331	329	7.2	7.3	41/4/01
R153Q	335	332	7.6	7.8	49/4/1
R153K	336	333	8.3	8.4	67/5/1
R160Q	335	333	7.4	7.6	46/4/1
R149Q + R153Q	335	333	7.6	7.8	50/4/1
R153Q + R160Q	335	333	8.1	8.2	59/5/1
R149Q + R153Q + R160Q	331	329	8.1	8.2	60/5/1
E146Q	336	333	7.6	7.8	50/5/1
D150N	336	334	7.9	8.0	55/4/1
D157N	335	332	7.7	8.0	53/4/1
E146A + R149A	335	333	7.3	7.4	42/4/1
R149A + D150A	331	329	8.2	8.2	64/6/1
R153A + D150A	331	329	8.1	8.2	63/5/1
R171Q	335	332	8.3	8.4	65/3/1
A175R	336	334	7.6	7.8	49/3/1

Diameter was determined by native gradient gel electrophoresis (GGE), and by gel filtration on a Superose 6PG column.



TABLE 3. Apparent kinetic constants for the reaction of LCAT with various rHDL consisting of PLPC/cholesterol/apoA-I complexes, prepared with wild-type and mutant apoA-I

ApoA-I Mutant in rHDL	Apparent $V_{max}$	Apparent $K_m$	Apparent $V_{max}/$ Apparent $K_m$
	<i>nmol/h·ml</i>	$\mu$ M	<i>nmol/ml·h/μM</i>
Wild type	256 ± 14	6.4 ± 0.7	40.0 ± 4.9
R149Q	19.1 ± 1.2	2.4 ± 0.7	8.0 ± 2.4
R153Q	22.5 ± 1.1	2.0 ± 0.4	11.3 ± 2.3
R153K	36.2 ± 4.5	5.2 ± 1.9	7.0 ± 2.7
R160Q	41.2 ± 2.8	10.5 ± 1.5	3.9 ± 0.6
R149Q + R153Q	10.8 ± 1.3	3.5 ± 1.9	3.1 ± 1.7
R153Q + R160Q	9.6 ± 1.2	6.6 ± 2.5	1.5 ± 0.6
R149Q + R153Q + R160Q	7.9 ± 0.3	5.8 ± 0.6	1.4 ± 0.2
E146Q	128.2 ± 3.5	2.2 ± 0.2	55.7 ± 11
D150N	113 ± 11	3.8 ± 1.3	30 ± 11
D157N	172.1 ± 6.6	3.0 ± 0.4	57.4 ± 8.0
E146A + R149A	19.7 ± 1.7	8.4 ± 1.7	2.3 ± 0.5
R149A + D150A	17.5 ± 1.3	4.4 ± 1.0	4.0 ± 0.9
R153A + D150A	15.7 ± 1.1	3.3 ± 1.0	4.8 ± 1.5
R171Q	268 ± 12	4.2 ± 0.5	63.8 ± 1.8
A175R	217.9 ± 6.5	3.1 ± 0.4	70.3 ± 9.3

The composition and diameter of the complexes are listed in Table 2.

a disruption of these salt bridges, as the R171Q mutation has only a limited effect on  $V_{max}$  while residue E179 is not conserved in the different apoA-I sequences.

The present study and previous results suggest a model for the activation of LCAT on discoidal rHDL. Jonas (29) previously proposed that LCAT associates with the upper face of the discoidal particle, and that this involves hydrophobic interactions with lipids, and/or more polar protein-protein interactions with apoA-I. Most published studies suggest that LCAT interacts directly with phospholipids, as the association constants are similar for lipid-protein complexes containing either apoA-I or apoA-II (30). These constants are of the same order of magnitude as measured for pure phospholipid vesicles. However, apoA-I specifically increases the apparent  $V_{max}$  for cholesterol esterification by LCAT. ApoA-IV and apoE are less reactive, whereas apoA-II suppresses LCAT activity on the complexes, by displacing other apolipoproteins (31, 32). Specific interactions between the enzyme and its cofactor might induce a conformational change in LCAT, which is required for full enzymatic activity. Such interactions probably have an electrostatic component, as LCAT has optimal activity at 150 mM NaCl (33). If so, R149, R153, and R160 in apoA-I could either form salt bridges with negative residues of LCAT, or hydrogen bonds with other polar residues of the enzyme (Fig. 6). As R149, R153, and R160 are located at the hydrophobic/hydrophilic boundary of the amphipathic helix, their side chains are in the right position to interact with a molecule of LCAT bound to the surface of the disc (Fig. 6). On a spherical HDL particle, “snorkeling” of the arginine side chains would enable similar interactions. In the crystal structure of apoA-I, the distribution of interhelical salt bridges is asymmetric (12). Most salt bridges are formed between antiparallel apoA-I molecules A and B, which probably represent the functional dimer, as also proposed in the model of Segrest et al. (13) for rHDL. Only this configuration is compatible with the orientation of the three mutated arginine residues toward the surface of the disc, in contrast to the A–C

and A–D dimers and to the picket-fence model of Phillips et al. (15).

In the  $\alpha/\beta$ -hydrolase model built for LCAT (34, 35), we previously proposed that the N-terminal part of helices  $\alpha$  3–4 (residues 115–132) and  $\alpha$  His (residues 385–401) might be involved in LCAT activation by apoA-I (36). This was based on the location of natural and LCAT mutants causing fish-eye disease, the biochemical phenotype of engineered mutations, and the similarities with cofactor activation processes in lipases. A direct interaction between these residues and apoA-I has not been demonstrated yet.

In conclusion, the data reported here are consistent with the belt model proposed for apoA-I in a discoidal lipid-apolipoprotein particle. They represent the first experimental link between the apoA-I conformation in the belt model and the functional activity of the apolipoprotein as a cofactor of LCAT. Mutations of R149, R153, and

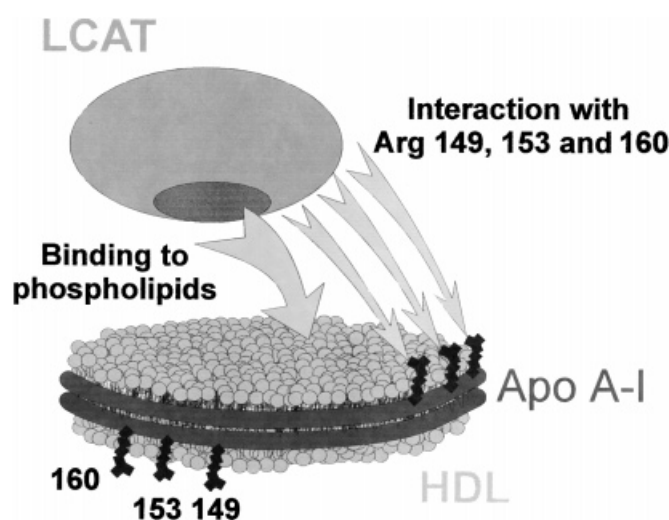



Fig. 6. Schematic representation of the proposed mode of interaction of LCAT with apoA-I arginine residues 149, 153, and 160, in a discoidal rHDL particle.

R160 of apoA-I do not inhibit LCAT activation through loss of internal salt bridges or decreased hydrophobic interactions with the phospholipid acyl chains. As demonstrated in this article, loss of activity can probably be ascribed to modification of polar interactions between apoA-I and LCAT. The role of the arginine cluster in the helical repeat 143–164 for the interaction of apoA-I with other ligands, such as cellular receptors or lipid transfer proteins, is currently being tested. 

Manuscript received 17 July 2000 and in revised form 29 August 2000.

## REFERENCES

- Frank, P. G., and Y. L. Marcel. 2000. Apolipoprotein A-I. Structure-function relationships. *J. Lipid Res.* **41**: 853–872.
- Yokoyama, S. 1998. Apolipoprotein-mediated cellular cholesterol efflux [erratum in *Biochim. Biophys. Acta.* 1998;1393: 222]. *Biochim. Biophys. Acta.* **1392**: 1–15.
- Acton, S., A. Rigotti, K. T. Landschulz, S. Xu, H. H. Hobbs, and M. Krieger. 1996. Identification of scavenger receptor SR-BI as a high density lipoprotein receptor. *Science.* **271**: 518–520.
- Bodzioch, M., E. Orso, J. Klucken, T. Langmann, A. Bottcher, W. Diederich, W. Drobnik, S. Barlage, C. Buchler, M. Porsch-Ozcurrence, W. E. Kaminski, H. W. Hahmann, K. Oette, G. Rothe, C. Aslanidis, K. J. Lackner, and G. Schmitz. 1999. The gene encoding ATP-binding cassette transporter 1 is mutated in Tangier disease. *Nat. Genet.* **22**: 347–351.
- Rust, S., M. Rosier, H. Funke, J. Real, Z. Amoura, J. C. Piette, J. F. Deleuze, H. B. Brewer, N. Duverger, P. Deneffe, and G. Assmann. 1999. Tangier disease is caused by mutations in the gene encoding ATP-binding cassette transporter 1. *Nat. Genet.* **22**: 352–355.
- Brooks-Wilson, A., M. Marcil, S. M. Clee, L. H. Zhang, K. Roomp, M. van Dam, L. Yu, C. Brewer, J. A. Collins, H. O. Molhuizen, O. Loubser, B. F. Ouellette, K. Fichter, K. J. Ashbourne-Excoffon, C. W. Sensen, S. Scherer, S. Mott, M. Denis, D. Martindale, J. Frohlich, K. Morgan, B. Koop, S. Pimstone, J. J. Kastelein, and M. R. Hayden. 1999. Mutations in ABC1 in Tangier disease and familial high-density lipoprotein deficiency. *Nat. Genet.* **22**: 336–345.
- Glomset, J. A. 1968. The plasma lecithin:cholesterol acyltransferase reaction. *J. Lipid Res.* **9**: 155–167.
- Brewer, H. B., Jr., T. Fairwell, A. LaRue, R. Ronan, A. Houser, and T. J. Bronzert. 1978. The amino acid sequence of human APOA-I, an apolipoprotein isolated from high density lipoproteins. *Biochem. Biophys. Res. Commun.* **80**: 623–630.
- Shoulders, C. C., and F. E. Baralle. 1982. Isolation of the human HDL apoprotein A1 gene. *Nucleic Acids Res.* **10**: 4873–4882.
- McLachlan, A. D. 1977. Repeated helical pattern in apolipoprotein-A-I. *Nature.* **267**: 465–466.
- Segrest, J. P., R. L. Jackson, J. D. Morrisett, and A. M. J. Gotto. 1974. A molecular theory of lipid-protein interactions in the plasma lipoproteins. *FEBS Lett.* **38**: 247–258.
- Borhani, D. W., D. P. Rogers, J. A. Engler, and C. G. Brouillette. 1997. Crystal structure of truncated human apolipoprotein A-I suggests a lipid-bound conformation. *Proc. Natl. Acad. Sci. USA.* **94**: 12291–12296.
- Segrest, J. P., M. K. Jones, A. E. Klone, C. J. Sheldahl, M. Hellinger, H. De Loof, and S. C. Harvey. 1999. A detailed molecular belt model for apolipoprotein A-I in discoidal high density lipoprotein. *J. Biol. Chem.* **274**: 31755–31758.
- Brasseur, R., J. De Meutter, B. Vanloo, E. Goormaghtigh, J. M. Ruysschaert, and M. Rosseneu. 1990. Mode of assembly of amphipathic helical segments in model high-density lipoproteins. *Biochim. Biophys. Acta.* **1043**: 245–252.
- Phillips, J. C., W. Wriggers, Z. Li, A. Jonas, and K. Schulten. 1997. Predicting the structure of apolipoprotein A-I in reconstituted high-density lipoprotein disks. *Biophys. J.* **73**: 2337–2346.
- Wald, J. H., E. Coormaghtigh, J. De Meutter, J. M. Ruysschaert, and A. Jonas. 1990. Investigation of the lipid domains and apolipoprotein orientation in reconstituted high density lipoproteins by fluorescence and IR methods. *J. Biol. Chem.* **265**: 20044–20050.
- Koppaka, V., L. Silvestro, J. A. Engler, C. G. Brouillette, and P. H. Axelsen. 1999. The structure of human lipoprotein A-I. Evidence for the “belt” model. *J. Biol. Chem.* **274**: 14541–14544.
- Sorci-Thomas, M. G., L. Curtiss, J. S. Parks, M. J. Thomas, M. W. Kearns, and M. Landrum. 1998. The hydrophobic face orientation of apolipoprotein A-I amphipathic helix domain 143–164 regulates lecithin:cholesterol acyltransferase activation. *J. Biol. Chem.* **273**: 11776–11782.
- Gilson, M. K., and B. Honig. 1988. Calculation of the total electrostatic energy of a macromolecular system: solvation energies, binding energies, and conformational analysis. *Proteins.* **4**: 7–18.
- Brooks, B. R., R. E. Bruccoleri, B. D. Olafson, D. J. States, S. Swaminathan, and M. Karplus. 1983. CHARMM: a program for macromolecular energy, minimization, and dynamics calculations. *J. Comput. Chem.* **4**: 187–217.
- Thompson, J. D., D. G. Higgins, and T. J. Gibson. 1994. CLUSTAL W: improving the sensitivity of progressive multiple sequence alignment through sequence weighting, position-specific gap penalties and weight matrix choice. *Nucleic Acids Res.* **22**: 4673–4680.
- Emmanuel, F., A. Steinmetz, M. Rosseneu, R. Brasseur, N. Gosset, F. Attenot, S. Cuine, S. Seguret, M. Latta, and J. C. Fruchart. 1994. Identification of specific amphipathic alpha-helical sequence of human apolipoprotein A-IV involved in lecithin:cholesterol acyltransferase activation. *J. Biol. Chem.* **269**: 29883–29890.
- Matz, C. E., and A. Jonas. 1982. Micellar complexes of human apolipoprotein A-I with phosphatidylcholines and cholesterol prepared from cholate-lipid dispersions. *J. Biol. Chem.* **257**: 4535–4540.
- Vanloo, B., J. Taveirne, J. Baert, G. Lorent, L. Lins, J. M. Ruysschaert, and M. Rosseneu. 1992. LCAT activation properties of apoA-I CNBr fragments and conversion of discoidal complexes into spherical particles. *Biochim. Biophys. Acta.* **1128**: 258–266.
- Bohm, G., R. Muhr, and R. Jaenicke. 1992. Quantitative analysis of protein far UV circular dichroism spectra by neural networks. *Protein Eng.* **5**: 191–195.
- Hill, J. S., X. Wang, S. Paranjape, D. Dimitrijevic, A. G. Lacko, and P. H. Pritchard. 1993. Expression and characterization of recombinant human lecithin:cholesterol acyltransferase. *J. Lipid Res.* **34**: 1245–1251.
- Vercaemst, R., A. Union, M. Rosseneu, I. De Craene, G. de Backer, and M. Kornitzer. 1989. Quantitation of plasma free cholesterol and cholesteryl esters by high performance liquid chromatography. Study of a normal population. *Atherosclerosis.* **78**: 245–250.
- Collet, X., Y. L. Marcel, N. Tremblay, C. Lazure, R. W. Milne, B. Perret, and P. K. Weech. 1997. Evolution of mammalian apolipoprotein A-I and conservation of antigenicity: correlation with primary and secondary structure. *J. Lipid Res.* **38**: 634–644.
- Jonas, A. 1998. Regulation of lecithin cholesterol acyltransferase activity. *Prog. Lipid Res.* **37**: 209–234.
- Bolin, D. J., and A. Jonas. 1994. Binding of lecithin:cholesterol acyltransferase to reconstituted high density lipoproteins is affected by their lipid but not apolipoprotein composition. *J. Biol. Chem.* **269**: 7429–7434.
- Labeur, C., G. Lambert, T. Van Cauteren, N. Duverger, B. Vanloo, J. Chambaz, J. Vandekerckhove, G. Castro, and M. Rosseneu. 1998. Displacement of apoA-I from HDL by apoA-II or its C-terminal helix promotes the formation of pre-beta1 migrating particles and decreases LCAT activation. *Atherosclerosis.* **139**: 351–362.
- Durbin, D. M., and A. Jonas. 1999. Lipid-free apolipoproteins A-I and A-II promote remodeling of reconstituted high density lipoproteins and alter their reactivity with lecithin:cholesterol acyltransferase. *J. Lipid Res.* **40**: 2293–2302.
- Jonas, A., J. L. Daehler, and E. R. Wilson. 1986. Anion effects on the reaction of lecithin-cholesterol acyltransferase with discoidal complexes of phosphatidylcholines · apolipoprotein A-I · cholesterol. *Biochim. Biophys. Acta.* **876**: 474–485.
- Peelman, F., N. Vinaimont, A. Verhee, B. Vanloo, J. L. Verschelde, C. Labeur, M. S. Seguret, N. Duverger, G. Hutchinson, J. Vandekerckhove, J. Tavernier, and M. Rosseneu. 1998. A proposed architecture for lecithin cholesterol acyl transferase (LCAT): identification of the catalytic triad and molecular modeling. *Protein Sci.* **7**: 587–599.
- Peelman, F., J. Vandekerckhove, and M. Rosseneu. 2000. Structure and function of lecithin cholesterol acyl transferase: new insights from structural predictions and animal models. *Curr. Opin. Lipidol.* **11**: 155–160.
- Vanloo, B., K. Deschuymere, F. Peelman, J. Taveirne, A. Verhee, C. Gouyette, C. Labeur, J. Vandekerckhove, J. Tavernier, and M. Rosseneu. 2000. Relationship between structure and biochemical phenotype of lecithin:cholesterol acyltransferase (LCAT) mutants causing fish-eye disease. *J. Lipid Res.* **41**: 752–761.